ELSEVIER

Experimental Thermal and Fluid Science 25 (2002) 659–676

Experimental Thermal and Fluid Science

www.elsevier.com/locate/etfs

Heat transfer measurements and correlations for air–water flow of different flow patterns in a horizontal pipe

Dongwoo Kim [a], Afshin J. Ghajar [b,*]

[a] *Samsung Electronics Company, Ltd., Suwon, Kyungki-Do, South Korea*
[b] *School of Mechanical and Aerospace Engineering, Oklahoma State University, Stillwater, OK 74078, USA*

Received 20 May 2001; received in revised form 30 September 2001; accepted 28 November 2001

Abstract

Heat transfer coefficients were measured and new correlations were developed for two-phase, two-component (air and water) heat transfer in a horizontal pipe for different flow patterns. Flow patterns were observed in a transparent circular pipe using an air–water mixture. Visual identification of the flow patterns was supplemented with photographic data, and the results were plotted on the flow regime map proposed by Taitel and Dukler and agreed quite well with each other. A two-phase heat transfer experimental setup was built for this study and a total of 150 two-phase heat transfer data with different flow patterns were obtained under a uniform wall heat flux boundary condition. For these data, the superficial Reynolds number ranged from 640 to 35,500 for the liquid and from 540 to 21,200 for the gas. Our previously developed robust two-phase heat transfer correlation for a vertical pipe with modified constants predicted the horizontal pipe air–water heat transfer experimental data with very good accuracy. Overall the proposed correlations predicted the data with a mean deviation of 1.0% and an rms deviation of 12%.

Keywords: Two-phase horizontal pipe flow; Flow patterns; Heat transfer correlations

1. Introduction

In many industrial applications, such as the flow of natural gas and oil in flowlines and wellbores, the knowledge of non-boiling two-phase, two-component (liquid and permanent gas) heat transfer is required. Numerous heat transfer coefficient correlations and experimental data for forced convective heat transfer during gas–liquid two-phase flow in vertical and horizontal pipes have been published over the past 40 years [1]. Of the two-phase heat transfer correlations that have been published, the majority were developed from limited experimental data and are only applicable to certain flow patterns and fluid combinations.

While most of these correlations were derived empirically based upon a small set of experimental data, others were based upon such concepts as the liquid acceleration model, the pressure drop model, and the separated flow model. Kim et al. [2] have presented descriptions of these concepts, and identified the correlations that were developed based on each concept. Their findings showed that there was no single correlation capable of predicting turbulent heat transfer with good predictive accuracy for all fluid combinations and different flow patterns in vertical pipes. In order to improve heat transfer predictions in vertical turbulent two-phase flow, regardless of fluid combination and flow pattern, Kim et al. [3] developed a new correlation (Eq. (1)). The improved correlation used a carefully derived heat transfer model which takes into account the appropriate contributions of both the liquid and gas phases using the respective cross-sectional areas occupied by the two phases.

$$\frac{h_{TP}}{(1-\alpha)h_L} = \left[1 + 0.27\left(\frac{x}{1-x}\right)^{-0.04}\left(\frac{\alpha}{1-\alpha}\right)^{1.21} \times \left(\frac{Pr_G}{Pr_L}\right)^{0.66}\left(\frac{\mu_G}{\mu_L}\right)^{-0.72}\right], \quad (1)$$

where h_L comes from the Sieder and Tate [4] equation and the parametric ranges were

* Corresponding author. Tel.: +1-405-744-5900; fax: +1-405-744-7873.
E-mail address: ghajar@ceat.okstate.edu (A.J. Ghajar).

0894-1777/02/$ - see front matter
PII: S0894-1777(01)00120-0

Nomenclature

A	cross-sectional area, m^2 or ft^2
C	constant value of the leading coefficient in Eq. (4) (see Table 3), dimensionless
c	specific heat at constant pressure, kJ/(kg K) or Btu/(lbm °F)
D	inside diameter of the tube, m or ft
F_{TD}	flow pattern transition parameter for wavy flow to annular or intermittent flow in [11] defined as $[(\rho_G V_{SG}^2)/((\rho_L - \rho_G)Dg\cos\Omega)]^{0.5}$, dimensionless
g	gravitational acceleration, m/s^2 or ft/s^2
h	heat transfer coefficient, $W/(m^2\ K)$ or Btu/(h ft^2 °F)
k	thermal conductivity, W/(m K) or Btu/(h ft °F)
K_{TD}	flow pattern transition parameter for stratified flow to wavy flow in [11] defined as $[(\rho_G V_{SG}^2\ V_{SL})/(\nu_L(\rho_L - \rho_G)g\cos\Omega)]^{0.5}$, dimensionless
L	length of the heated test section, m or ft
m	constant exponent value on the quality ratio term in Eq. (4) (see Table 3), dimensionless
$\dot{m}$	mass flow rate, kg/s or lbm/h
n	constant exponent value on the void fraction ratio term in Eq. (4) (see Table 3), dimensionless
Nu	Nusselt number ($=hD/k$), dimensionless
P	mean system pressure, Pa or psi
p	constant exponent value on the Prandtl number ratio term in Eq. (4) (see Table 3), dimensionless
Pr	Prandtl number ($=c\mu/k$), dimensionless
q	constant exponent value on the viscosity ratio term in Eq. (4) (see Table 3), dimensionless
Re	Reynolds number ($=\rho VD/\mu_B$), dimensionless
Re_L	liquid in-situ Reynolds number ($=4\dot{m}_L/\pi\sqrt{1-\alpha}\mu_L D$), dimensionless
T	temperature, °C or °F
T_{TD}	flow pattern transition parameter for intermittent (slug or plug) flow to bubbly flow in [11] defined as $[(-(dP/dz)_L)/((\rho_L - \rho_G)g\cos\Omega)]^{0.5}$, where $-(dP/dz)_L$ is calculated from [11], dimensionless
V	average velocity in the test section, m/s or ft/s
X	Martinelli parameter $[=((1-x)/x)^{0.9}(\rho_G/\rho_L)^{0.5}(\mu_L/\mu_G)^{0.1}]$, dimensionless
x	flow quality $[=\dot{m}_G/(\dot{m}_G+\dot{m}_L)]$, dimensionless

Greek symbols

α	void fraction $[=A_G/(A_G+A_L)]$, dimensionless
Ω	angle of inclination between the pipe axis and the horizontal, degree
μ	dynamic viscosity, Pa s or lbm/(h ft)
ν	kinematic viscosity, m^2/s or ft^2/s
ρ	density, kg/m^3 or lbm/ft^3

Subscripts

B	bulk
CAL	calculated
EXP	experimental
G	gas
L	liquid
MIX	gas–liquid mixture
TP	two-phase
SG	superficial gas
SL	superficial liquid
W	wall

$$4000 < Re_{SL} < 1.26\times10^5,$$

$$8.4\times10^{-6} < \left(\frac{x}{1-x}\right) < 0.77,$$

$$0.01 < \left(\frac{\alpha}{1-\alpha}\right) < 18.61,$$

$$1.18\times10^{-3} < \left(\frac{Pr_G}{Pr_L}\right) < 0.14,$$

$$3.64\times10^{-3} < \left(\frac{\mu_G}{\mu_L}\right) < 0.02.$$

It should be noted that the exponent value on the parameter $[x/(1-x)]$ in Eq. (1) has a very small magnitude (0.04) for the sets of experimental data used in our previous study [3]. However, even with a small exponent, this term still appears to play an important role, since complete elimination of the parameter yielded substantial under predictions. In calculation of the single-phase heat transfer coefficient (h_L) required by the use of Sieder and Tate [4] correlation in Eq. (1), the following relationship was used to evaluate the in-situ Reynolds number (liquid phase) rather than the superficial Reynolds number (Re_{SL}) as commonly used in the correlations of the available literature (see [1]):

$$Re_L = \left(\frac{\rho VD}{\mu_B}\right)_L = \frac{4\dot{m}_L}{\pi\sqrt{1-\alpha}\mu_L D}. \tag{2}$$

In the development of Eq. (1), the values of the void fraction (α) were directly taken from the original experimental data [5–7]. These α values were calculated by the original investigators based on the equation provided by Chisholm [8] and the suggested equation was

$$\alpha = \left[1 + \left(\frac{V_G}{V_L}\right)\left(\frac{1-x}{x}\right)\frac{\rho_G}{\rho_L}\right]^{-1}. \tag{3}$$

The suggested correlation (Eq. (1)) for a vertical pipe predicted very well the heat transfer coefficient for the 255 experimental data points for water–air, silicone–air, water–helium, and water–freon 12, having an overall mean deviation of 2.54%, an rms deviation of 12.78%, and a deviation range of −64.71% to 39.55% [3].

The main purpose of this study was to extend our vertical pipe two-phase heat transfer studies and develop heat transfer correlations which can be applied to two-phase heat transfer data in a horizontal pipe with different flow patterns. In order to achieve this goal successfully, a two-phase heat transfer experimental setup was built and additional horizontal flow pattern data were obtained since very limited experimental data (one set of slug flow data from [9] and one set of annular flow data from [10]) are available from the open literature. Visual identification of the flow patterns was supplemented with photographic data, and the results were plotted on the flow regime map proposed by Taitel and Dukler [11]. The results of comparing the observed flow patterns and the calculated flow patterns on the Taitel and Dukler map indicated that both agreed quite well with each other.

A total of 150 two-phase heat transfer data with different flow patterns were measured in a horizontal pipe under a uniform wall heat flux boundary condition. For these data, the superficial Reynolds number ranged from 640 to 35,500 for the liquid and from 540 to 21,200 for the gas. Since slug data in a horizontal pipe were available from the open literature, this study emphasized more on slug flow heat transfer data. Finally, our previously developed robust two-phase heat transfer correlation for a vertical pipe [3] with modified constants was used to predict the air–water heat transfer data in a horizontal pipe.

2. Experimental setup and data reduction

A schematic diagram of the overall experimental setup for heat transfer measurements is shown as Fig. 1. The test section is a horizontal seamless 316 schedule S10 stainless steel circular tube [1.097 in. (2.79 cm) I.D., 1.315 in. (3.34 cm) O.D., and $L/D = 100$]. In order to apply uniform wall heat flux boundary condition to the test section, copper plates were silver soldered to the inlet and exit of the test section. The uniform wall heat flux boundary condition was maintained by a Lincoln SA-750 welder. The entire length of the test section was rapped using fiberglass pipe wrap insulation, followed by a thin polymer vapor seal to prevent moisture penetration.

In order to develop various two-phase flow patterns (by controlling the flow rates of gas and liquid) such as stratified, wavy, slug, bubbly, or annular flow a two-phase gas and liquid mixer was constructed. The mixer consisted of a perforated copper tube [0.24 in. (0.61 cm) O.D.] inserted into the liquid stream by means of a tee and a compression fitting (see Fig. 2) as suggested by Ewing et al. [12]. The end of the copper tube was silver-soldered. Four 1/16 in. (1.6 mm) holes were positioned at 90° intervals around the perimeter of the tube and this pattern was repeated at eight equally spaced axial

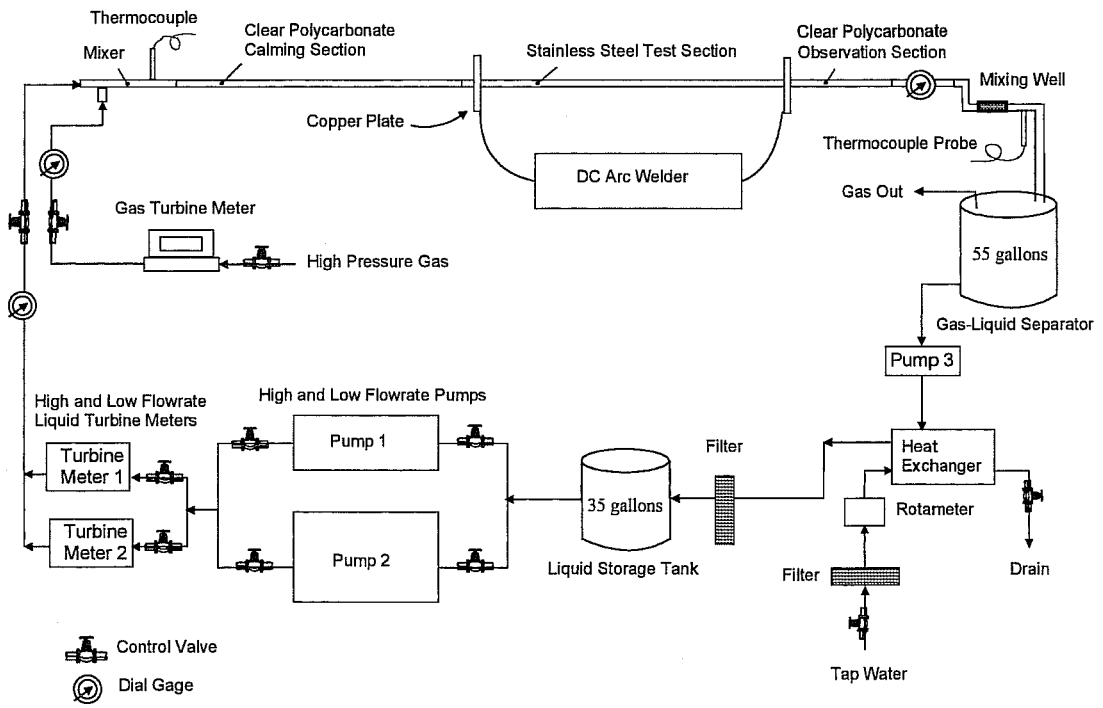

Fig. 1. Schematic diagram of the experimental setup.

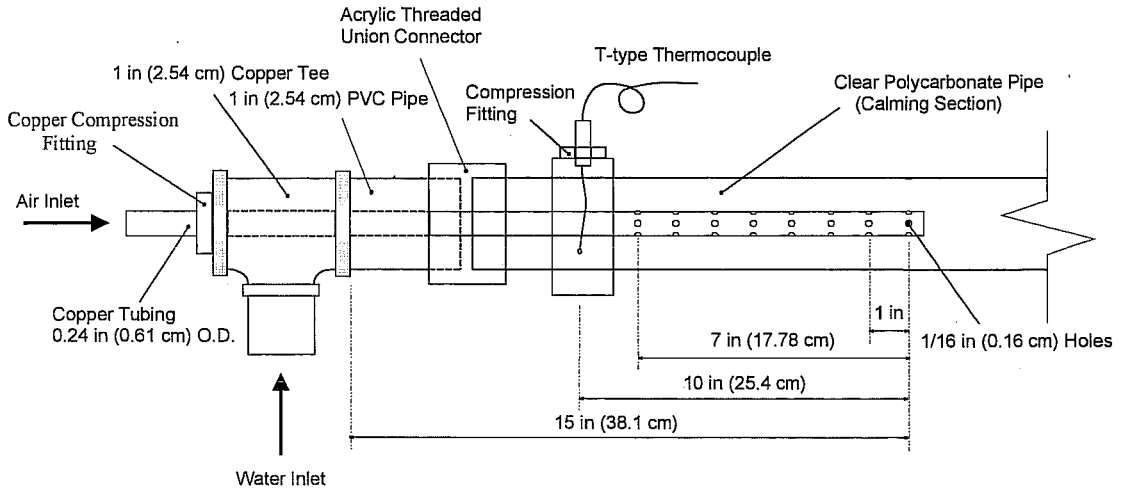

Fig. 2. Schematic diagram of the gas–liquid mixer.

locations along the length of the copper tube as shown in Fig. 2. The two-phase flow leaving mixer entered the transparent calming section.

The calming section [clear polycarbonate pipe with 1 in. (2.54 cm) I.D. and $L/D = 88$] serves as a flow developing and turbulence reduction device, and flow pattern observation section. One end of the calming section was connected to the test section with an acrylic flange and the other end of the calming section was connected to the gas–liquid mixer. The test section, the calming section, and the observation section (refer to Fig. 1) were carefully leveled for reducing the effect of inclination on horizontal flow measurements.

T-type thermocouple wires were cemented with Omegabond 101, an epoxy adhesive with high thermal conductivity and electrical resistivity, to the outside wall of the stainless steel test section. The length of each thermocouple wire was 12 in. (30.48 cm) + 1.5 times the outside diameter of the tube. This length was long enough to eliminate thermocouple error due to lead wire heat conduction in the temperature gradient field [13]. OMEGA EXPP-T-20-TWSH extension wires were used for relay to the data acquisition system. Thermocouples were placed on the outer surface of the tube wall at uniform intervals of 10 in. (25.4 cm) from the entrance to the exit of the test section (see Fig. 3). There were 10

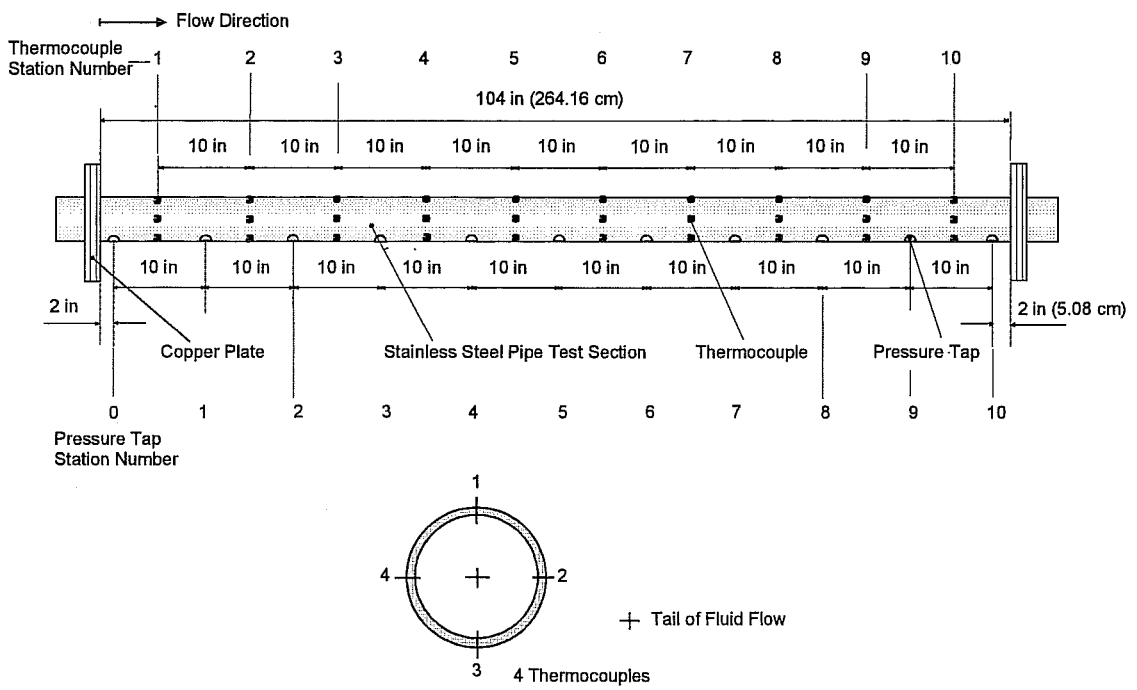

Fig. 3. Thermocouple and pressure tap locations along the test section.

thermocouple stations in the test section. All stations had four thermocouples, and they are labeled looking at the tail of the fluid flow with peripheral location number one being at the top of the tube, two being 90° in the clockwise direction, three at the bottom of the tube, and four being 90° from the bottom in the clockwise sense. All the thermocouples were monitored with a Cole–Parmer MAC-14 datalogger with 96 channels. The thermocouple readings were averaged over a user chosen length of time (typically 60 s) before the heat transfer measurements were actually recorded. The average system stabilization time period was from 30 to 60 min after the system attained steady state. The inlet liquid and gas temperatures were measured by OMEGA TT-T-30 T-type thermocouple wires, and the exit bulk temperature was measured by an OMEGA TJ36-CPSS-14U-12 thermocouple probe inserted after the mixing well. Calibration of thermocouples and thermocouple probes showed that they were accurate within ±0.5 °C [14]. The operating pressures inside the experimental setup were monitored with three dial type pressure gages (see Fig. 1).

To ensure a uniform fluid bulk temperature at the exit of the test section, a mixing well was utilized. An alternating polypropylene baffle type static mixer for both gas and liquid phases was used. This mixer provided an overlapping baffled passage forcing the fluid to encounter flow reversal and swirling regions. The mixing well was placed below the clear Polycarbonate observation section (after the test section), and before the gas–liquid separator liquid storage tank (refer to Fig. 1). Since the cross-sectional flow passage of the mixing was substantially smaller than the test section, it had the potential of increasing the system back-pressure. Thus, in order to reduce the potential back-pressure problem, which might affect the flow pattern inside of the test section, the mixing well was placed below and after the test section and the clear observation sections. The outlet bulk temperature was measured immediately after the mixing well. An ITT Standard model BCF 4036 one shell and two tube pass heat exchanger was used to cool the test fluid to an allowable and steady-state bulk temperature.

In order to measure the volumetric flow rate of the gas supplied to the system flow line, a 0.25 in. (6.35 mm) NPT flowmeter was used. The amount of gas supplied to the system was monitored through a 3-digit LCD display. The output voltage generated from the flowmeter was linear over the entire range and connected to an A/D board. In order to calculate gas density and the mass flow rate of the supplied gas, the gas absolute pressure was measured.

Two flow meters, which are an impeller flow meter [0.05–5 GPM (11.36×10^{-3} to 1.136 m^3/h)] and a turbine flow meter [3–9 GPM (0.86 to 2.04 m^3/h)] were connected to an OMEGA DPF700 6-digit rate meter/totalizer equipped with an analog output board, measured the volumetric flow rate of distilled water feeding into the test loop. The frequency generated from those flow meters was measured by the rate meter/totalizer and converted to voltage signal fed into the A/D board.

The heat transfer measurements at uniform wall heat flux boundary condition were carried out by measuring the local outside wall temperatures at 10 stations along the axis of the tube and the inlet and outlet bulk temperatures in addition to other measurements such as the flow rates of gas and liquid, room temperature, voltage drop across the test section, and current carried by the test section. The peripheral heat transfer coefficient (local average) and the Nusselt number thereafter were calculated based on the knowledge of the pipe inside wall surface temperature and inside wall heat flux obtained from a data reduction program developed exclusively for this type of experiments [15]. The local average peripheral values for inside wall temperature, inside wall heat flux, and heat transfer coefficient were then obtained by averaging all the appropriate individual local peripheral values at each axial location. The computer program used a finite-difference formulation to determine the inside wall temperature and the inside wall heat flux from measurements of the outside wall temperature, the heat generation within the pipe wall, and the thermophysical properties of the pipe material (electrical resistivity and thermal conductivity). In these calculations, axial conduction was assumed negligible, but peripheral and radial conduction of heat in the tube wall were included. In addition, the bulk fluid temperature was assumed to increase linearly from the inlet to outlet.

The reliability of the flow circulation system and of the experimental procedures was checked by making several single-phase calibration runs with distilled water. The single-phase heat transfer experimental data were checked against the well established single-phase heat transfer correlations of Colburn [16], Sieder and Tate [4], Gnielinski [17], and Ghajar and Tam [18] in the Reynolds number range from 3000 to 30,000.

Fig. 4(a) shows the comparison of experimental Nusselt numbers with the calculated Nusselt numbers by using the Colburn [16] correlation. The lower recommended Reynolds number range of the Colburn correlation is 10,000. Among the 31 single-phase experimental data points, a total of 23 data points ($Re > 8000$) were used to predict the Colburn correlation. Within the recommended range of Reynolds number, most of the 23 data points fell within a ±10% deviation band as can be seen from Fig. 4(a), which shows a very good agreement between the experimental Nusselt numbers and the predictions from the Colburn correlation. A maximum deviation of 16.99% and a minimum deviation of −5.49%, and a mean deviation of 5.76% with an rms deviation of 8.55% is achieved by using the Colburn correlation.

Since the lower recommended Reynolds number was 10,000 by the Sieder and Tate [4] correlation, a total of

23 data points having Reynolds numbers greater than 8000 were used for the Sieder and Tate correlation. As shown in Fig. 4(b), the results were very similar to those produced by the Colburn [16] correlation due to the fact that the Sieder and Tate correlation added the viscosity ratio term to the Colburn correlation. From this aspect, we can see that the viscosity ratio term is not very significant for single-phase water heat transfer. For the comparisons shown in Fig. 4(b) there was a maximum deviation of 16.45%, a minimum deviation of −6.75%, and a mean deviation of 4.81% with an rms deviation of 8.08%. Most of data points fell into a ±10% deviation band, which showed a very good Nusselt number comparison.

The Gnielinski [17] correlation covered transitional and fully turbulent ($3000 \leqslant Re \leqslant 10^6$) flows. Thus, the 13 transitional and 18 fully turbulent flow heat transfer data points could be examined. As shown in Fig. 4(c), the comparison of the experimental Nusselt numbers with the calculated ones using the Gnielinski correlation showed very good agreement between the experimental and the predicted values. The results with the Gnielinski correlation have a maximum deviation of 13.82% and a minimum deviation of −8.18%, and a mean deviation of 1.20% with an rms deviation of 6.49%. Most of the data fell into a ±10% deviation band as shown in Fig. 4(c).

The Ghajar and Tam [18] correlation applies several limitations such as the ratios of the axial length to pipe inside diameter, the Reynolds number, the Prandtl number, and the ratio of bulk to wall viscosities. Among those limitations, the Reynolds number and the viscosity ratio were considered since the rest of the limitations were sufficiently satisfied. A total of 16 data points ($1.06 \leqslant \mu_b/\mu_w \leqslant 1.151, Re \geqslant 6000$) were predicted with the Ghajar and Tam correlation. The results shown in Fig. 4(d) indicate that the experimental Nusselt numbers agreed well with the predictions of the Ghajar and Tam correlation. Most of data fell into the ±10% deviation band, having a maximum deviation of 6.91%, a minimum deviation of −14.36%, and a mean deviation of

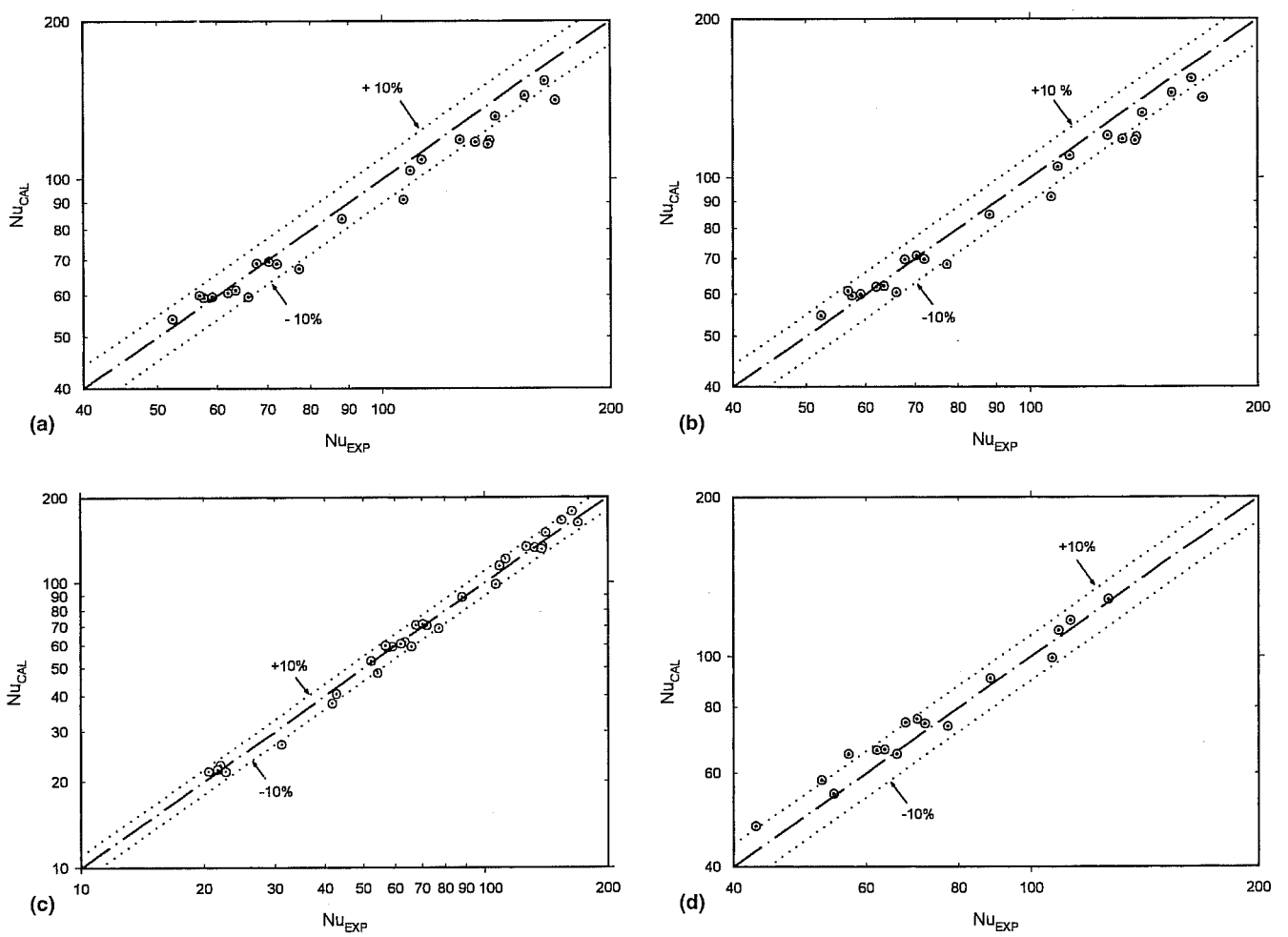

Fig. 4. (a) Comparison of Colburn [16] correlation with single-phase experimental data from current study (23 points); (b) comparison of Sieder and Tate [4] correlation with single-phase experimental data from current study (23 points); (c) comparison of Gnielinski [17] correlation with single-phase experimental data from current study (31 points); (d) comparison of Ghajar and Tam [18] correlation with single-phase experimental data from current study (16 points).

−4.28% with an rms deviation of 6.90%. From this result, it can be concluded that the current data are reasonably accurate since the proven Ghajar and Tam correlation predictions agree very well with the data presented herein.

In most instances, the experimental results were well within ±10% of the predicted results. The uncertainty analyses of the overall experimental procedures using the method of Kline and McClintock [19] showed that there is a maximum of 9% uncertainty for heat transfer coefficient calculations. Experiments under the same conditions were conducted periodically to ensure the repeatability of the results. The maximum difference between the duplicated experimental runs were within ±10%. More details of experimental setup and data reduction procedures can be found from [14].

3. Presentation of flow patterns

Due to the multitude of flow patterns and the various interpretations accorded to them by different investigators, no uniform procedure exists at present for describing and classifying them. However, in recent years, some attempts have been made to standardize the description and terminology of the flow patterns [11,20–23]. In this study, the flow pattern identification for the experimental data was based on the procedures suggested by Taitel and Dukler [11], Breber et al. [20], and visual observation as appropriate.

All observations for the flow pattern judgements were made at two locations, just before the test section (about $L/D = 93$ in the calming section) and right after the test section. Leaving the liquid flow rate fixed, flow patterns were observed for various air flow rates. The liquid flow rate was then adjusted and the process was repeated. If the observed flow patterns differed at the two locations of before and after the test section, experimental data was not taken and the flow rates of gas and liquid were readjusted for consistent flow pattern observations. In our flow pattern studies, for the size of the pipe diameter used (2.54 cm), the effects of the wettability of our horizontal transparent pipe on the observed flow patterns of air–water two-phase flows in the pipe were considered insignificant. According to Barnea et al. [24] these effects become significant for small diameter pipes (<12.5 mm), where the surface tension is the dominant factor. Table 1 shows a summary of the two-phase flow pattern experimental data taken. This table shows the flow patterns observed; number of data points taken in each flow pattern; minimum, maximum, and averaged values of the mass flow rates of liquid and gas along with their superficial velocities and Reynolds numbers; Martinelli parameter (X); temperature and pressure of gas–liquid mixture; two-phase pressure drop along the test section (ΔP); supplied gas pressure (P_G); void fraction (α); and Prandtl numbers of liquid and gas. Some of the basic flow patterns (stratified, wavy, and slug) in a horizontal pipe and several transitional flow patterns (wavy–slug, annular–wavy, annular–bubbly, annular–bubbly–slug, and bubbly–slug) were observed. Those visually observed flow patterns were photographed by means of a high speed still camera using three high intensity discharge lamps (one 300 W and two 150 W lamps) without the aid of a stroboscope.

Representative photographs of the various flow patterns that were observed are given in Fig. 5. Fig. 5(a) illustrates the observed stratified flow pattern in which liquid flowing in the bottom of the pipe was separated from gas in the upper portion of the pipe by a relatively smooth interface. Fig. 5(b) shows the observed wavy flow pattern. After the flow rate and/or the quality was increased for the stratified flow pattern, the interface became unstable, whereupon the interface became wavy. For the wavy flow pattern, the velocity of the gas was sufficient to cause waves to form but not enough to cause the waves to reach the top of the pipe surface. In Fig. 5(c), those waves caused by the gas flow, under conditions where the velocity of the gas was sufficient for the rapid wave growth, reached the top of the inside pipe surface. This type of flow was categorized as a wavy–slug transitional flow pattern.

In Fig. 5(d), as the liquid rate was increased, the liquid level rose, and waves were formed so that their crests spanned the entire width of the pipe, effectively forming large slug-type bubbles. The slugs of gas flowing along the tube, because of their buoyancy, tended to skew toward the upper portion of the pipe. In Fig. 5(e), a wavy type of liquid film at the bottom side of the pipe together with the liquid annulus along the inside pipe wall were observed. At high gas velocities and moderate liquid flow rates, there was insufficient liquid flow to maintain and form a liquid bridge, and the liquid in the wave was swept up around the tube to form a liquid annulus with some entrainment. For such conditions, buoyancy effects tended to thin the liquid film on the top portion of the pipe wall and thicken it at the bottom. This transitional type of flow pattern was classified as that from the wavy to the annular transition flow pattern.

In Fig. 5(f), a liquid film annulus together with a frothy type of bubbly slugs were observed. Under these conditions, buoyancy effects still tended to thin the liquid film on the top portion of the pipe wall and thicken it at the bottom, resulting in a slightly thicker liquid film at the bottom side of the pipe wall than the liquid film at the top. With relatively high gas and liquid flow rates, a much thinner liquid annulus than that of Fig. 5(f) with a frothy type of bubbly slugs was observed in Fig. 5(g). Under this condition, the gas flow was invariably turbulent, and strong lateral Reynolds stresses and the shear resulting from secondary flows might serve to

Table 1
Summary of the two-phase flow pattern experimental data

	$\dot{m}_L$ (lbm/h)	V_{SL} (ft/s)	Re_{SL}	$\dot{m}_G$ (lbm/h)	V_{SG} (ft/s)	Re_{SG}	X	T_{MIX} (°F)	P_{MIX} (psi)	ΔP (in H_2O)	P_G (psi)	α	Pr_L	Pr_G
Stratified flow pattern (13 *data points*)														
Min.	86.72	0.07	709.38	1.58	1.08	539.26	0.34	78.80	0.23	0.03	0.01	0.74	5.18	0.71
Max.	187.76	0.15	1359.7	12.53	6.49	4272.3	2.92	89.96	1.17	0.17	5.67	0.91	5.99	0.71
Avg.	124.11	0.10	974.82	6.35	3.75	2169.9	1.08	86.43	0.67	0.09	1.81	0.85	5.42	0.71
Wavy flow pattern (9 *data points*)														
Min.	84.57	0.07	628.69	12.63	6.47	4341.9	0.21	77.54	0.25	0.37	4.71	0.85	5.26	0.71
Max.	319.23	0.26	2424.0	32.61	8.21	11179.	0.79	88.70	1.38	1.37	25.77	0.92	6.09	0.71
Avg.	184.78	0.15	1369.3	23.97	7.68	8206.6	0.48	81.25	0.62	0.69	16.43	0.89	5.81	0.71
Wavy–slug flow pattern (7 *data points*)														
Min.	317.18	0.26	2276.9	9.20	5.38	3113.0	0.96	78.08	0.39	1.08	2.71	0.75	5.36	0.71
Max.	977.10	0.80	7153.4	20.26	7.47	6982.2	2.30	87.26	0.86	2.58	12.32	0.84	6.05	0.71
Avg.	525.98	0.43	4026.7	13.88	6.56	4736.1	1.59	83.35	0.55	1.88	6.30	0.80	5.64	0.71
Slug flow pattern (46 *data points*)														
Min.	319.36	0.26	2425.0	1.61	1.10	546.76	1.64	78.08	0.24	0.10	0.03	0.29	5.38	0.71
Max.	5461.9	4.47	43068.	20.82	7.46	7087.5	36.85	86.90	7.16	18.15	16.54	0.80	6.05	0.71
Avg.	2046.9	1.67	15534.	8.51	4.20	2895.9	9.49	82.94	1.68	5.09	4.35	0.59	5.67	0.71
Wavy–annular flow pattern (14 *data points*)														
Min.	82.31	0.07	662.55	42.63	8.13	14430.	0.13	78.62	0.82	0.51	37.34	0.77	5.26	0.71
Max.	925.90	0.76	7000.8	77.88	9.51	26361.	1.50	88.70	3.73	9.27	69.82	0.94	6.01	0.71
Avg.	380.63	0.31	2882.3	59.28	8.93	20093.	0.57	83.59	1.87	4.04	53.12	0.87	5.63	0.71
Annular–bubbly or annular–bubbly–slug flow pattern (12 *data points*)														
Min.	1243.7	1.02	9564.4	41.95	8.16	14308.	1.67	79.16	3.04	8.60	37.36	0.60	5.52	0.71
Max.	3785.5	3.10	29480.	76.41	9.60	25996.	4.27	84.92	10.50	24.52	66.67	0.74	5.96	0.71
Avg.	2155.5	1.76	16220.	59.61	8.88	20248.	2.74	81.93	6.06	16.09	53.66	0.68	5.75	0.71
Bubbly–slug flow pattern (12 *data points*)														
Min.	905.99	0.74	6762.9	24.31	7.08	8291.9	1.74	78.44	1.56	4.55	17.58	0.52	5.39	0.71
Max.	4888.0	4.00	35707.	79.57	9.65	27070.	9.07	86.72	12.86	24.36	70.75	0.76	6.02	0.71
Avg.	3242.8	2.65	23971.	41.36	8.08	14052.	4.95	80.69	6.94	16.94	36.07	0.61	5.84	0.71

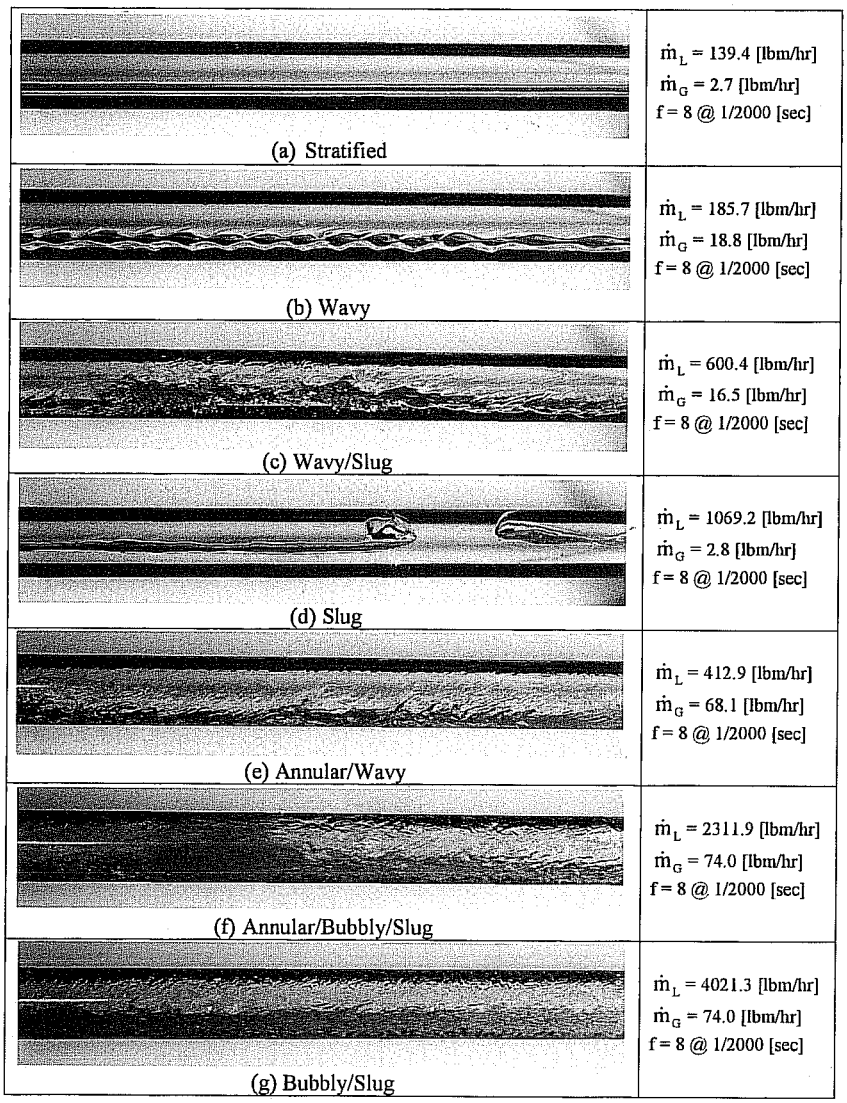

Fig. 5. Photographs of representative flow patterns.

distribute the liquid more evenly around the tube perimeter against the tendency of gravity to stratify the flow. This type of observed flow pattern was classified as a bubbly–slug transitional flow pattern.

In order to build a solid flow pattern criteria, measured experimental data having a variety of different flow patterns judged by appropriate visual observation along with the description of Carey [25] were plotted on the flow pattern map of [11]. In Fig. 6, observed stratified flow pattern data points were compared with their calculated positions on the Taitel and Dukler map. All of the observed data points (13 data points) were below the stratified wavy (SW) curve. Thus, we can conclude from this result that the observed flow pattern is stratified flow pattern.

Fig. 7 shows the comparisons of the Taitel and Dukler map with the observed wavy flow pattern data. Fig. 7(a) shows that some of the observed wavy flow pattern data were on the stratified wavy (SW) curve. Thus, the comparison of the observed flow pattern data and the K_{TD} curve did not provide enough information for accurate flow pattern judgement. Fig. 7(b) shows the calculated F_{TD} values of the wavy to annular and wavy to intermittent (plug or slug) transitions for the observed wavy flow pattern data. All of the observed data points (13 data points) were below the F_{TD} transition line. Therefore, from this result, we can confirm that the observed flow pattern is the wavy flow pattern.

Experimentally observed wavy–slug transition flow pattern data is compared with the calculated position on the Taitel and Dukler map in Fig. 8. As can be seen from this figure, three of seven data points were just below the line of wavy to annular and wavy to intermittent (plug or slug) transitions, and three of seven data points for F_{TD} values were close to the transition line of wavy to intermittent (plug or slug) transition curve. Thus, we can

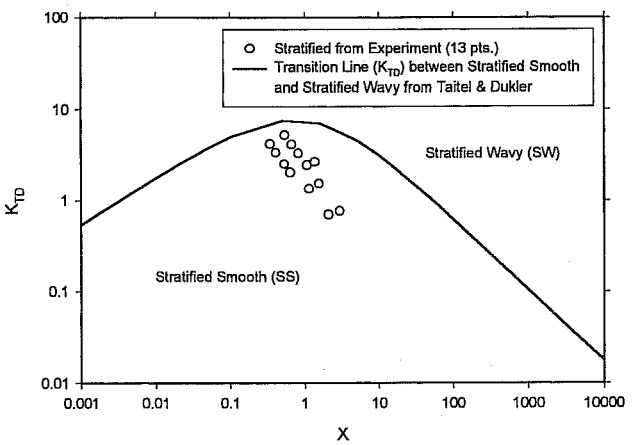

Fig. 6. Comparison of Taitel and Dukler [11] map with stratified flow pattern data.

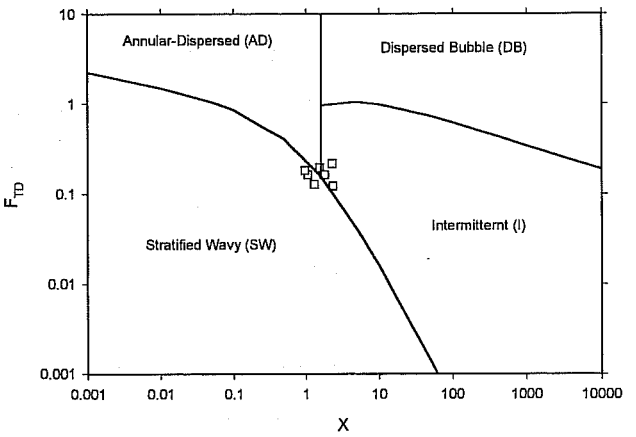

Fig. 8. Comparison of Taitel and Dukler [11] map with wavy–slug transitional flow pattern data.

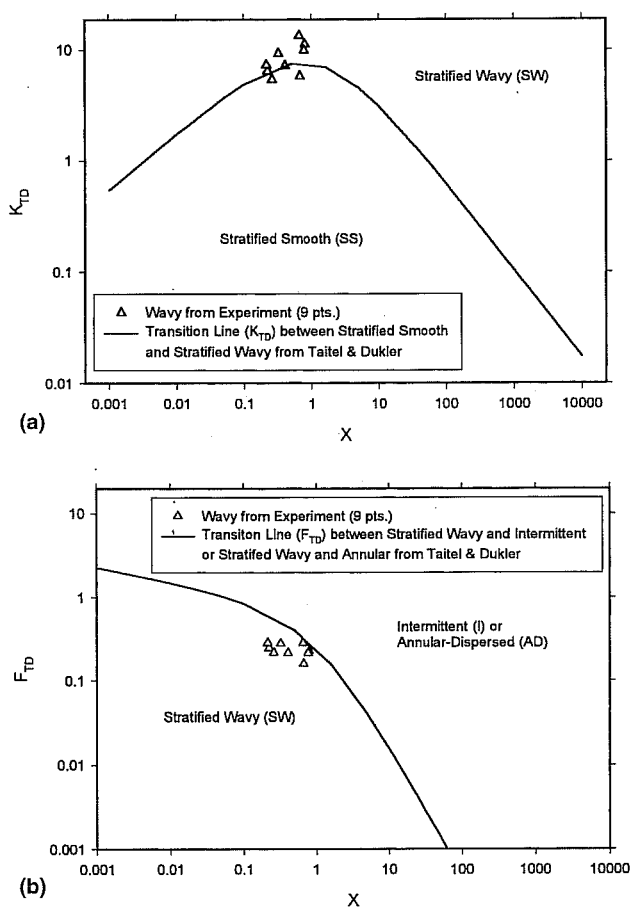

Fig. 7. Comparisons of the Taitel and Dukler [11] map with wavy flow pattern data.

conclude that the observed flow pattern is wavy to intermittent (plug or slug) transition flow pattern.

Comparisons of Taitel and Dukler map with experimentally observed slug flow pattern data are plotted in Fig. 9. Fig. 9(a) shows that some of the observed slug flow pattern data were just below the line of stratified flow to wavy flow transition values, K_{TD}, and others were above the K_{TD} line. Thus, we could not judge the observed flow pattern from this comparison. The observed flow pattern was compared with the wavy to annular and wavy to intermittent transition line of F_{TD} in Fig. 9(b). Again, some of the observed slug flow pattern data were just below the line of wavy to annular and wavy to intermittent flow pattern transition values of F_{TD}, and others were above the F_{TD} line. Thus, we could not judge the observed flow pattern from this comparison. Fig. 9(c) shows the comparison of the observed flow pattern with the intermittent (slug or plug) to dispersed bubbly flow pattern transition (T_{TD}) and intermittent to annular dispersed flow pattern transition ($X = 1.6$). As can be seen from this comparison, all of the observed flow pattern data were below the line of intermittent to dispersed bubble transition, T_{TD}, and greater than the line value of the intermittent to annular dispersed flow transition ($X = 1.6$). Therefore, we can conclude that the observed flow pattern is slug flow pattern. Similar procedures were applied to the other observed flow pattern data. Based on the results of these comparisons, all of the observed flow pattern data agreed well with the flow pattern map of Taitel and Dukler [11].

Experimentally observed flow pattern data were plotted using their corresponding values of mass flow rates of air and water in Fig. 10. Shaded lines in the diagonal direction show possible flow pattern transitions. Under the conditions of small amounts of air and water flow rates, stratified flow patterns were observed. At moderate gas flow rates with low liquid flow rates, wavy flow patterns were observed. Also, with low liquid flow rates together with relatively high air flow rates, annular–wavy transitional flow patterns were observed. Next, with moderate to relatively high liquid flow rates together with low to moderate air flow rates, slug flow patterns were observed.

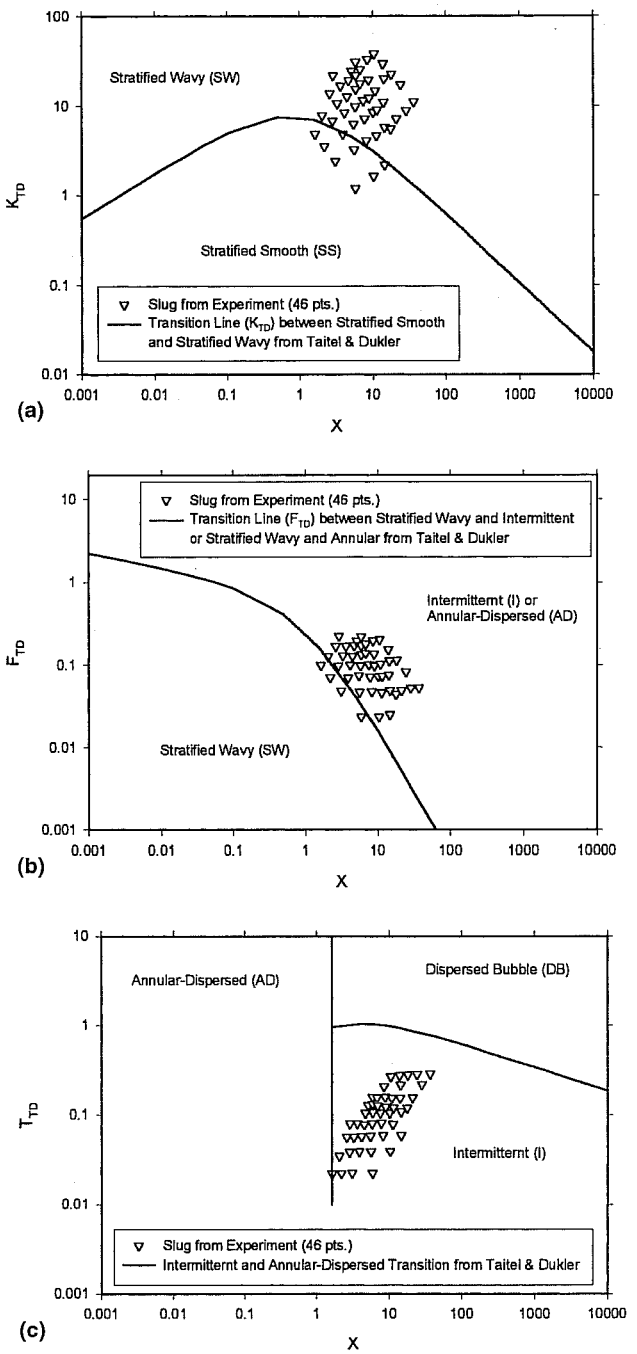

Fig. 9. Comparisons of Taitel and Dukler [11] map with slug flow pattern data.

With relatively moderate mass flow rates of both air and water, wavy–slug transitional flow patterns were observed. With relatively high liquid flow rates mixed with high air flow rates, either bubbly–slug or annular–bubbly–slug transitional flow patterns were observed. However, it was very difficult to clearly distinguish the location of either bubbly–slug or annular–bubbly–slug flow patterns in Fig. 10.

Table 2 shows the minimum and maximum values of air and water mass flow rates according to the different flow pattern classifications. These minimum and maximum values are based on the rectangular shapes which were plotted in Fig. 10. The rectangles were constructed by connecting more than three data points at which the same flow patterns were observed. With these rectangular shapes, a desired flow pattern can be easily controlled by taking the amounts of air and liquid inside the minimum and maximum straight lines in the rectangle. In this way the ambiguity in judging the right flow pattern can be avoided.

Table 2 also shows the number of experimental data points that have been obtained for the two-phase heat transfer experiments. Those numbers are based on the area occupied in Fig. 10. Due to the large area and the shape of the slug flow pattern regime in Fig. 10, two rectangles were plotted on this figure for slug flow and two different minimum and maximum values of air and liquid mass flow rates are suggested in Table 2. It should be mentioned that, due to the small area of the wavy–slug flow pattern and the difficulty of clearly controlling the mass flow rates of air and liquid based on the irregular shape of the boundaries in Fig. 10, no number of data points for the wavy–slug flow pattern was assigned in Table 2. The suggested limits for the mass flow rates of air and water in the wavy–slug flow pattern in Table 2 are somewhat arbitrary and the mass flow rates of air and water should be carefully adjusted in order to generate clear wavy–slug transitional flow patterns. Also, due to the difficulty of applying low wall heat flux to the test section (<350 A), no heat transfer measurement in the stratified flow pattern was obtained. Since, both of the gas and liquid flow rates are relatively quite small in this case, there was the strong possibility of boiling due to the continuous increase of the top surface temperature of the inside pipe wall. This situation could cause damage to the test section. Thus, no heat transfer measurement for the stratified flow pattern was assigned in Table 2.

4. Two-phase heat-transfer results

Fig. 11 shows the variation of mean heat transfer coefficient parametrically versus superficial Reynolds numbers (Re_{SG} and Re_{SL}) for all of the air–water data obtained in this study. From this figure, it can be seen that generally, as the gas superficial Reynolds number (Re_{SG}) increases for a fixed liquid superficial Reynolds number (Re_{SL}), the heat transfer coefficient increases. Some of the previous researchers also observed an increase in two-phase heat transfer as the gas Reynolds number increased for a fixed liquid Reynolds number. Zaidi and Sims [26] observed from the results of their two-phase heat transfer measurements in a vertical pipe that h_{TP} generally increased as the air flow rate was increased for each fixed liquid flow rate. Also, the increase

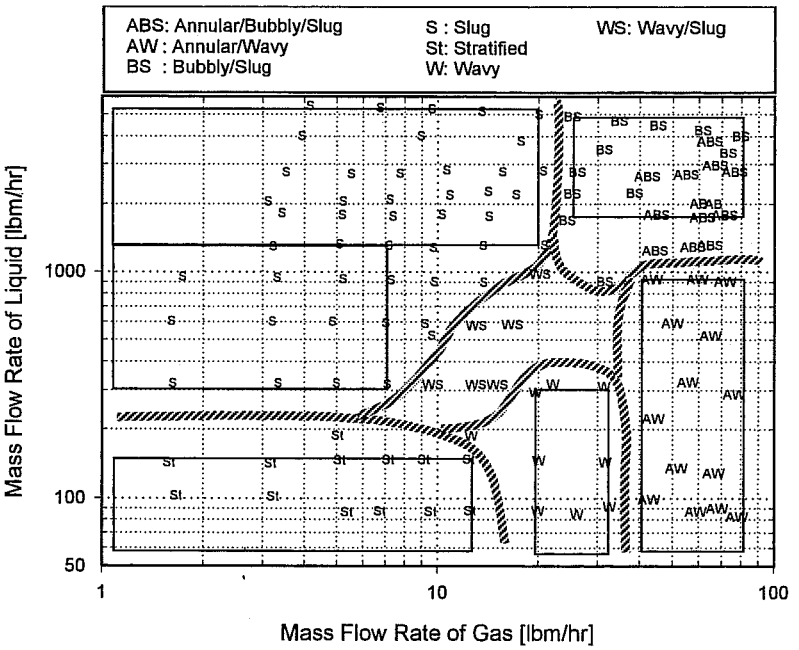

Fig. 10. Observed flow pattern data versus the corresponding mass flow rates of air and water.

Table 2
Minimum and maximum values of the air and water mass flow rates according to the different flow patterns and number of experimental data points taken

$\dot{m}_G$ (lbm/h)		$\dot{m}_L$ (lbm/h)		Expected flow pattern	Prospective number of data points
Min.	Max.	Min.	Max.	All of the flow patterns	150
0	12	0	147	Stratified	–
0	7	300	1300	Slug	25
0	20	1300	5460	Slug	30
20	32	0	310	Wavy	20
10	30	300	800	Wavy–slug	–
24	80	1080	4890	Bubbly–slug or annular–bubbly–slug	35
43	80	0	925	Annular–wavy	40

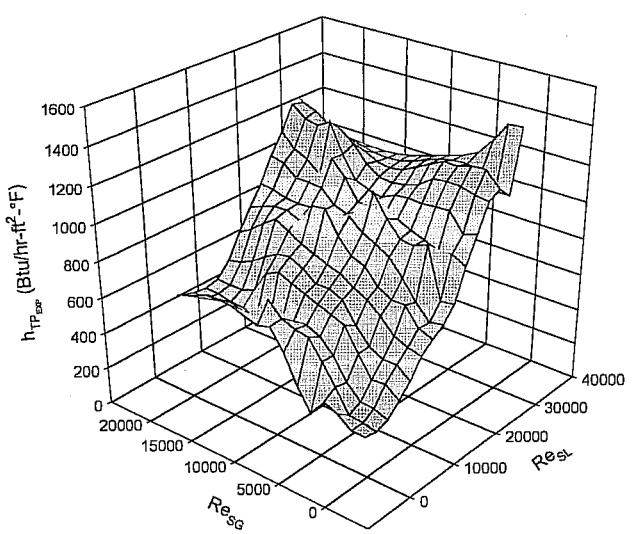

Fig. 11. Variation of mean heat transfer coefficient with Re_{SL} and Re_{SG} for the air–water data obtained in this study.

in h_{TP} was more significant at low Re_{SL} than at high Re_{SL}. They explained the increase in h_{TP}, as suggested by Kudirka et al. [27], by the turbulence level already present in the liquid stream. At low liquid flow rates, the turbulence level in the liquid stream is small before being introduced into the gas stream. The introduction of the gas phase into the liquid stream increases the turbulence level which results in a high heat transfer coefficient. However, at high Re_{SL}, the turbulence level is already high and the effect of the gas-phase in h_{TP} is not that pronounced.

Kudirka et al. [27] observed the increase in h_{TP} caused by the addition of a gas phase into liquid flow from their air–water and air–ethylene glycol mixtures in a vertical pipe. They discussed the reasons for those increases in terms of the following possible mechanisms: liquid and mixture velocity increase due to the addition of the gas phase; increased turbulence and mixing action in the main stream due to continuous interaction of the two

phases; and increased turbulence near the heated wall caused by gas bubbles, resulting in disturbances and a decrease in the effective thickness of the viscous boundary sublayer by the fact that the eddies, present in the wake of the rising bubbles, penetrate in the viscous sublayer. Groothuis and Hendal [28] mentioned in comparing their own air–oil and air–water results that the influence of air on heat transfer was most pronounced at the lowest Reynolds numbers because air would be more effective in promoting turbulence there.

Ravipudi and Godbold [29] found from their experimental data of air–water and air–toluene mixtures in a vertical pipe that the introduction of air into the liquid increased the heat transfer coefficient substantially due to the reduction of the effective thickness of the viscous sublayer. They also found that h_{TP} increased, reached a maximum and then decreased. The maximum in h_{TP} was observed to be in the transition zone between annular flow and mist flow. They explained that the highly turbulent motion of the gas–liquid mixture with increasing amounts of air caused randomly distributed dry spots to appear on the wall, thereby decreasing the heat transfer rate. Also, they attributed the decrease in h_{TP} at high Re_{SG} to the following. First, the outlet liquid temperature decreased due to the mass transfer from liquid to air. Next, h_{TP} did not increase in proportion to the increase in the temperature gradient. Finally, the measurement of two-phase mixture temperature was difficult.

From Fig. 11, we can also observe that there exists a maximum value of h_{TP} as Re_{SG} increases for a fixed Re_{SL}. For Re_{SL} greater than about 30,000, h_{TP} reached a maximum, then h_{TP} decreased as more air was added into the test section. Previously, Pletcher and McManus [30] also observed from air–water annular flow experiments in a horizontal pipe that h_{TP} passes through a maximum for a given water flow rate and then decreases as the air flow rate increases. They explained this trend as follows. As the air flow rate increases, a countering mechanism comes into play which tends to reduce the heat transfer coefficients by depressing the final exit equilibrium temperature. This occurs since, as the ratio of air flow rate to water flow rate increases, more and more evaporation is possible. At some air flow rate, this latter mechanism begins to dominate. They also suggested that the decrease in h_{TP} was due to liquid entrainment at the higher air rates.

Fig. 12 shows the trend in h_{TP} as a function of the values of Re_{SG} and Re_{SL} for each different flow pattern. For the wavy flow pattern, Fig. 12(a), h_{TP} increases relatively linearly as Re_{SG} increases for a fixed liquid Re_{SL}. However, h_{TP} is rather independent of Re_{SL}. The h_{TP} magnitude increased by more than five times as Re_{SG} increased from 7000 to 10,000. From these results, it can be concluded that the influence of air on heat transfer is most pronounced at the lowest Re_{SL} because air would be more effective in promoting turbulence there. Similar observations were also made by Zaidi and Sims [26], Kudirka et al. [27], and Groothuis and Hendal [28].

For the wavy to annular transitional flow pattern, Fig. 12(b), a relative maximum in h_{TP} exists as Re_{SG} increases for a fixed liquid Re_{SL}. This mechanism can be explained by the following reasons, suggested by Ravipudi and Godbold [29] and Pletcher and McManus [30]: the outlet liquid temperature decreased due to mass transfer from the liquid to the air; the measurement of the two-phase mixture temperature was difficult; or the liquid entrainment at the relatively higher air rates reduced the exit mixture bulk temperature.

For the slug flow pattern (Fig. 12(c)) and the slug to bubbly or annular–bubbly–slug transitional flow pattern (Fig. 12(d)), h_{TP} generally increases as either Re_{SG} or Re_{SL} increases. However, at high Re_{SL}, the effect of gas-phase in h_{TP} is not pronounced since the turbulence level of the liquid is already high.

Limited experimental data (one set of slug flow data from [9] and one set of annular flow data from [10]) are available from the open literature. Slug flow air–water heat transfer experimental data in a horizontal pipe has been obtained from the current study and from [9]. (Due to the limited capacity of the current study's experimental setup, no pure annular flow pattern data could be achieved.) It is desirable to see how well the two slug flow experimental data sets could be compared. However, direct comparison with King's [9] experimental data was impossible due to the fact that King's experimental range of gas and liquid mass flow rates was much higher than those of this study, and his experiments were conducted under a uniform wall temperature boundary condition (steam heated test section) rather than a uniform wall heat flux boundary condition. Therefore, the next best approach would be to compare the results of predictions of these two data sets by previously recommended heat transfer correlations.

Fig. 13 shows the comparison of the predictions of Kim et al.'s [3] vertical pipe correlation (Eq. (1)) with the 150 horizontal pipe experimental data points from the current study and the 21 slug flow data points from King's [9] horizontal pipe experiments. As shown in this figure, the previously recommended correlation (Eq. (1)) for a vertical pipe regardless of flow pattern and fluid combination predicted the heat transfer coefficients quite well for the bubbly–slug and bubbly–slug–annular transitional flow data, which can be obtained in both vertical and horizontal pipes. All of those predictions were within a ±30% deviation band. However, the trend of predictions for the heat transfer coefficients in wavy flow or wavy–annular transitional flow patterns were not correctly predicted. Since complete separation between phases of gas and liquid occurred in the wavy flow and wavy–annular transitional flow patterns with relatively small flow rates of air and water, the heat transfer

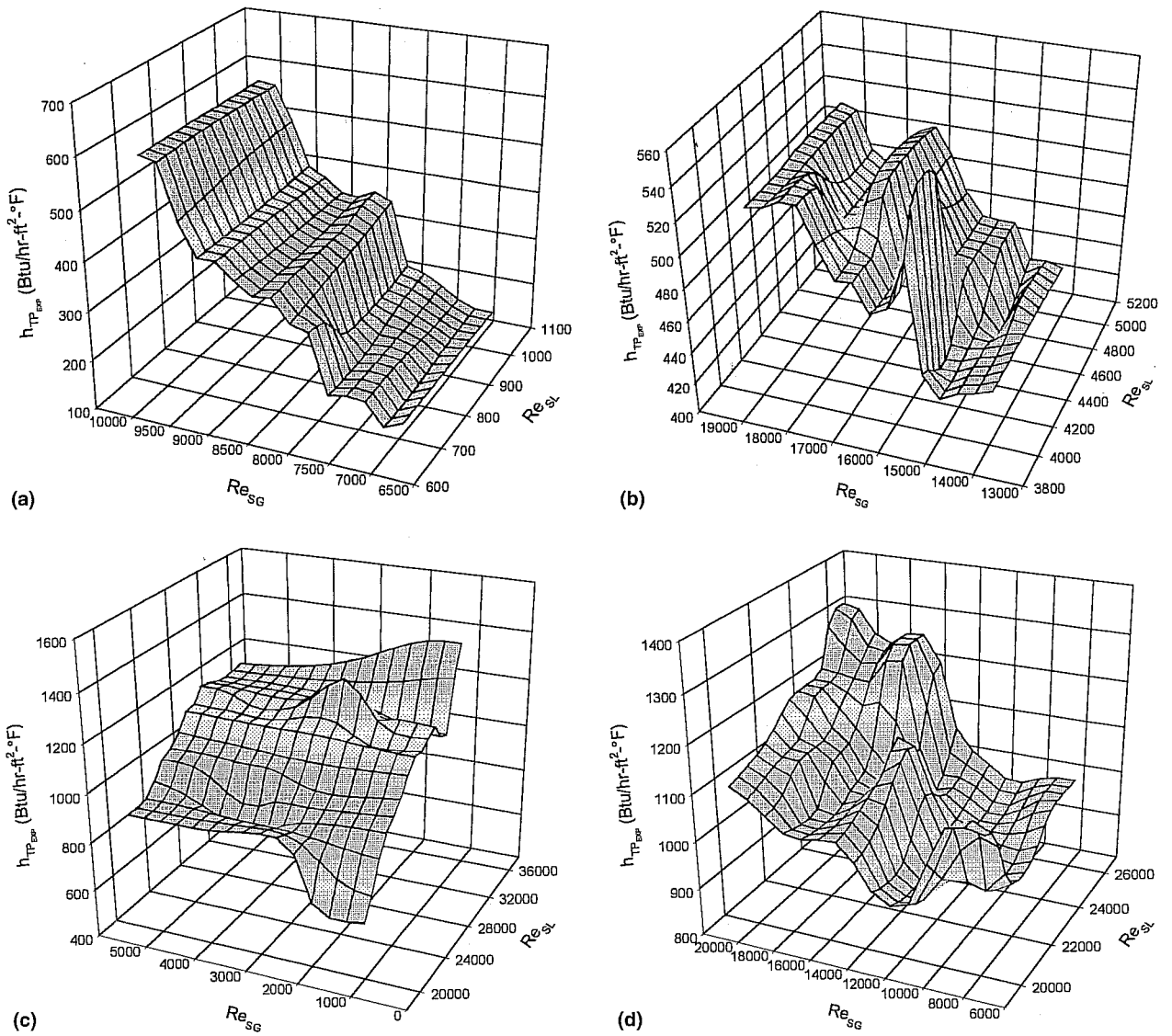

Fig. 12. (a) Air–water two-phase heat transfer coefficient for the wavy flow pattern (20 data points); (b) air–water two-phase heat transfer coefficient for the wavy–annular transitional flow pattern (41 data points); (c) air–water two-phase heat transfer coefficients in slug flow pattern (53 data points); (d) air–water two-phase heat transfer coefficients in bubbly–slug or annular–bubbly–slug transitional flow pattern (36 data points).

mechanism in a horizontal pipe appears to be quite different from the heat transfer mechanism in a vertical pipe, as can be seen from the heat transfer predictions for wavy flow and wavy–annular transitional flow patterns in Fig. 13.

It is interesting to note that there are similarities in the distribution of King's predicted results and the current study's slug flow data as shown in Fig. 13. Also, the predictions for both slug data sets are close to the ±30% deviation band. Thus, the experimental data in only slug flow and in bubbly–slug transitional flow can be accurately predicted by the previously recommended correlation for a vertical pipe with minor adjustment of its constants.

Fig. 14 shows a comparison of the predictions of the general form of the two-phase heat transfer correlation ([3, Eq. (13)]) with modified constants for the 21 slug experimental data points of [9] and 89 experimental data points of the current study. Table 3 also shows the general form of the two-phase heat transfer correlation (Eq. (4)) previously recommended by Kim et al. [3]. In order to predict those experimental data accurately, the values of the leading coefficient (C) and the exponents on the quality ratio term (m) and the void fraction term (n) were modified from the previously recommended values (Eq. (1)) using the least-squares method. Since the Prandtl number ratio term and the viscosity ratio term are typically used to represent large variation in physical properties and the influence of the properties of different fluids, the original vertical flow exponents p and q were retained (see Table 3). This new recommended correlation yielded a mean deviation of 0.36%,

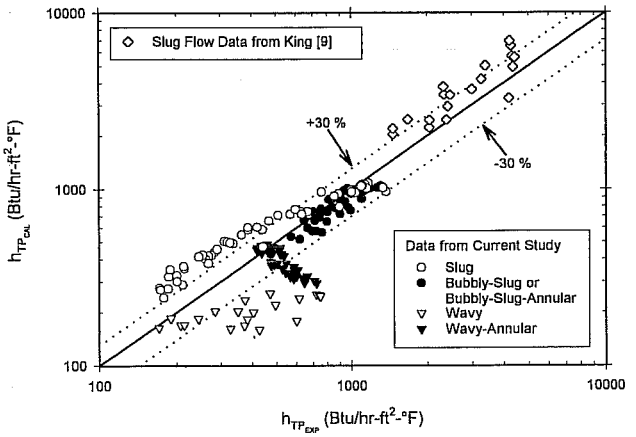

Fig. 13. Comparison of Kim et al. [3] vertical pipe correlation with current horizontal pipe experimental data (150 points) and King's [9] horizontal pipe data (21 points).

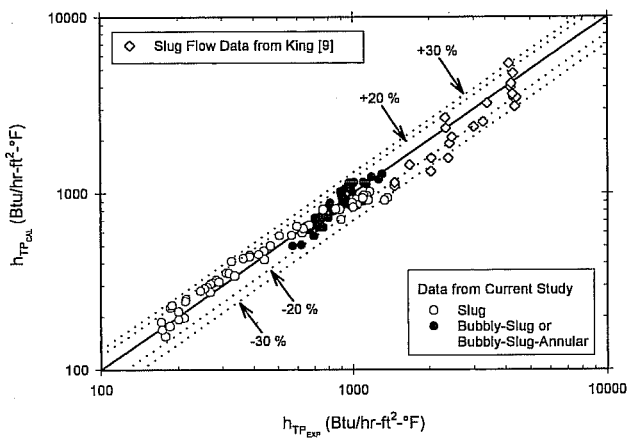

Fig. 14. Comparison of recommended correlation for slug flow and bubbly–slug or annular–bubbly–slug transitional flow with current horizontal pipe experimental data (89 points) and King's [9] horizontal pipe data (21 points).

an rms deviation of 12.29%, and a deviation range of −25.17% to 31.31%. About 92% of the slug flow or its transitional flow experimental data (82 data points) were predicted with less than ±20% deviation. This new recommended correlation also predicted the slug flow data from [9] with a mean deviation of 12.79%, an rms deviation of 20.78%, and a deviation range of −31.13% to 35.13%.

A similar procedure was used for our other experimental data with wavy and wavy–annular transitional flow patterns. Table 3 shows the summary of the values of the leading coefficient (C) and exponents (m, n, p, q) in the recommended general form (Eq. (4)) of the two-phase heat transfer correlation, the prediction results for each different flow pattern, and the range of each parameter in the general form of the correlation. From this table, the following two important observations were made.

First, since the ranges of Re_{SL} for the wavy flow or wavy–annular transitional flow are lower than the suggested Re_{SL} range for the vertical heat transfer correlation, it was necessary for all of the five constants, the leading coefficient (C) and exponents (m, n, p, q) including the Prandtl number ratio term (p) and the viscosity ratio term (q), to be modified from the previously recommended values in order to predict h_{TP} accurately. From this result, it can be concluded that the effects of the Prandtl number ratio term and the viscosity ratio term on h_{TP} in laminar flow of the liquid ($Re_{SL} < 4000$) are more pronounced than their effects on h_{TP} in the turbulent flow regime. However, since the above observation is based on limited air–water experimental data in a horizontal pipe, this observation should be further verified by comparing the results with additional experimental data for several different fluid combinations as they become available.

Second, since the range of the parameters for the wavy flow pattern are considerably different than those for the other flow patterns (see Table 3), this leads to the much larger values for the constants recommended to be used in the heat transfer correlation for this flow pattern. In particular, the difference between the relative magnitudes of the gas and liquid flow rates in this flow pattern (wavy) in comparison to other flow patterns (see Table 3) is mostly responsible for this large increase in the heat transfer correlation constants.

Graphical prediction results in wavy–annular transitional flow and wavy flow are also provided in Fig. 15. From this figure, the improved predictions by the new values in Table 3 may be observed as compared with the previously recommended correlation for a vertical pipe (Eq. (1)) shown in Fig. 13. As can be seen from this figure, the trends in h_{TP} for wavy–annular transitional flow and wavy flow are now correctly predicted (in contrast to the results in Fig. 13). 100% of the wavy–annular transition flow data (41 data points) and 80% of the wavy flow data (16 data points out of 20) were predicted within less than ±20%. Fig. 16 shows the predictions based on the recommended constants given in Table 3 for all of the flow pattern data from the current study. The overall deviation range of the prediction is from −25% to 34%, the overall mean deviation is about 1%, and the overall rms deviation is about 12%. 93% of all of the data (139 data points out of 150) from current study were predicted within less than ±20%.

5. Practical significance

Two-phase flow occurs frequently in the processing industries, and the design of such equipment as condensers, heat exchangers, and reactors depends on a detailed knowledge of two-phase flow to predict heat transfer in conjunction with the appropriate flow pattern.

Table 3
Summary of the values of the leading coefficient (C) and exponents (m, n, p, q) in the recommended heat transfer coefficient correlation (h_{TP}), the results of prediction, and the parameter range of the correlation

General form of the two-phase heat transfer coefficient correlation:

$$h_{TP} = (1-\alpha)h_L\left[1 + C\left(\frac{x}{1-x}\right)^m\left(\frac{\alpha}{1-\alpha}\right)^n\left(\frac{Pr_G}{Pr_L}\right)^p\left(\frac{\mu_G}{\mu_L}\right)^q\right] \quad (4)$$

Experimental data	Value of C and exponents (m, n, p, q).					Mean dev. (%)	rms dev. (%)	Number of data within ±20%	Range of dev. (%)	Range of parameter				
	C	m	n	p	q					Re_{SL}	$\left(\frac{x}{1-x}\right)$	$\left(\frac{\alpha}{1-\alpha}\right)$	$\left(\frac{Pr_G}{Pr_L}\right)$	$\left(\frac{\mu_G}{\mu_L}\right)$
Slug and Bubbly–slug Bubbly–slug–annular 89 data points from current study	2.86	0.42	0.35	0.66	−0.72	0.36	12.29	82	−25.17 and 31.31	2468 and 35,503	6.9×10^{-4} and 0.03	0.36 and 3.45	0.102 and 0.137	0.015 and 0.028
Slug 21 data points from King [9]						12.79	20.78	10	−31.13 and 35.13	22,500 and 119,000	7.1×10^{-4} and 0.11	0.34 and 7.55	0.23 and 0.25	0.041 and 0.044
Wavy–annular 41 data points from current study	1.58	1.40	0.54	−1.93	−0.09	1.15	3.38	41	−12.77 and 19.26	2163 and 4985	0.05 and 0.13	3.10 and 4.55	0.10 and 0.11	0.015 and 0.018
Wavy 20 data points from current study	27.89	3.10	−4.44	−9.65	1.56	3.60	16.49	16	−19.79 and 34.42	636 and 1829	0.08 and 0.25	4.87 and 8.85	0.102 and 0.107	0.016 and 0.021
All of the data points for current study 150 data points	See above for the values for each flow pattern					1.01	12.08	139	−25.17 and 34.42	636 and 35,503	6.9×10^{-4} and 0.25	0.36 and 8.85	0.102 and 0.137	0.015 and 0.028

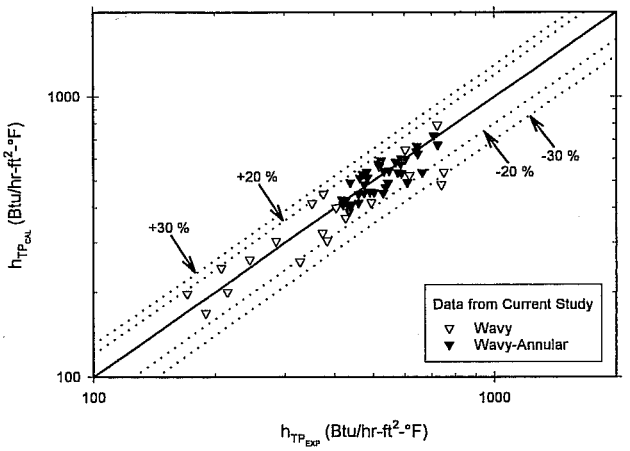

Fig. 15. Comparison of recommended correlations with wavy flow data (20 points) and wavy–annular transitional flow data (41 points) from current study.

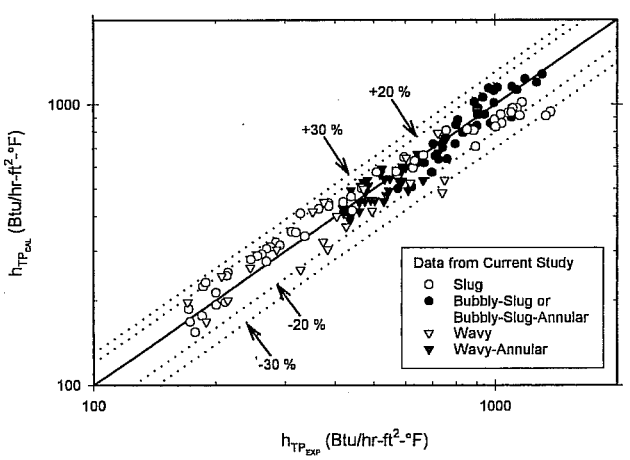

Fig. 16. Comparison of recommended correlations with data from current study (150 points).

The flow of a liquid and a permanent gas (usually referred to as two-phase, two-component flow) also involves a wide range of industrial applications such as the flow of natural gas in pipelines, oil wells and many chemical processes. Providing information on the heat transfer coefficient in the fluids in wellbores and pipelines to predict the occurrence of paraffin deposition on the pipe wall is another example of the importance of two-phase flow in oil and gas production systems, which has received considerable attention in recent years due to the growing need for more economical design and optimization of operating conditions. The heat transfer correlations provided in this study can be used to assist the multiphase system designer in predicting the two-phase heat transfer coefficients along a horizontal or vertical circular pipe with uniform heat flux in several different flow patterns regardless of the fluid combinations.

6. Summary and conclusions

This study was undertaken to develop new two-phase heat transfer correlations which can be applied to air–water non-boiling two-phase heat transfer data in a horizontal pipe for different flow patterns. In order to achieve this goal successfully, a reliable two-phase heat transfer experimental setup was built, and additional experimental data for different flow patterns were obtained. Based on the procedures of the flow pattern identification suggested by Taitel and Dukler [11] and visual observation as appropriate, a new flow pattern identification map was suggested. The results of comparing the observed flow patterns and the calculated flow patterns on the Taitel and Dukler map indicated that both agreed quite well with each other.

Based on the air–water two-phase heat transfer results of this study, the trends of the mean heat transfer coefficients (h_{TP}) for wavy and slug flow patterns and wavy–annular, slug–bubbly, and annular–bubbly–slug transitional flow patterns were presented in Figs. 11 and 12. Since the introduction of the gas phase into the liquid stream increases the turbulence level and mixing action in the main stream due to the continuous interaction of the two phases, the heat transfer coefficient generally increases as Re_{SG} increases for a fixed Re_{SL}. However, there exists a maximum value of h_{TP} as Re_{SG} increases for a fixed Re_{SL}. For the wavy to annular transitional flow pattern, a relative maximum in h_{TP} exists as Re_{SG} increases. This mechanism can be explained based on the following reasons. First, due to liquid entrainment at the relatively higher air flow rates, the exit mixture bulk temperature decreases. Second, due to mass transfer from the liquid to the air, the outlet liquid temperature decreases.

In order to predict the new air–water heat transfer experimental data in a horizontal pipe, our previously recommended correlation (Eq. (1)) for two-phase heat transfer in a vertical pipe with modified constants predicted 150 experimental data with good accuracy (mean deviation of 1% and an rms deviation of about 12%) as shown in Table 3 and Fig. 16.

In our future work, we plan to continue this study by investigating the development of a correlation which is robust enough to span all or most of the fluid combinations, flow patterns, flow regimes (laminar and turbulent), and pipe orientations (vertical, inclined, and horizontal). This will require the inclination angle and other experimental parameters to be added to our proposed heat transfer correlation.

Acknowledgements

The authors gratefully acknowledge the financial support provided by the Oklahoma State University (OSU) Foundation.

References

[1] D. Kim, A.J. Ghajar, R.L. Dougherty, V.K. Ryali, Comparison of twenty two-phase heat transfer correlations with seven sets of experimental data, including flow pattern and tube orientation effects, Heat Transfer Eng. 20 (1) (1999) 15–40.

[2] D. Kim, A.J. Ghajar, R.L. Dougherty, Development of improved two-phase two-component pipe flow heat transfer correlations from existing correlations and published data, Presented at the 5th ASME/JSME Joint Thermal Engineering Conference, San Diego, CA, Paper No. AJTE-99-6122, March 15–19, 1999.

[3] D. Kim, A.J. Ghajar, R.L. Dougherty, Robust heat transfer correlation for turbulent gas–liquid flow in vertical pipes, J. Thermophys. Heat Transfer 14 (4) (2000) 574–578.

[4] E.N. Sieder, G.E. Tate, Heat transfer and pressure drop of liquids in tubes, Ind. Eng. Chem. 28 (12) (1936) 1429–1435.

[5] M.A. Aggour, Hydrodynamics and heat transfer in two-phase two-component flow, Ph.D. Thesis, Mechanical Engineering Department, University of Manitoba, Winnipeg, MB, Canada, 1978.

[6] M.M. Vijay, A study of heat transfer in two-phase two-component flow in a vertical tube, Ph.D. Thesis, Mechanical Engineering Department, University of Manitoba, Winnipeg, MB, Canada, 1978.

[7] K.S. Rezkallah, Heat transfer and hydrodynamics in two-phase two-component flow in a vertical tube, Ph.D. Thesis, Mechanical Engineering Department, University of Manitoba, Winnipeg, MB, Canada, 1986.

[8] D. Chisholm, Research note: void fraction during two-phase flow, J. Mech. Eng. Sci. 15 (3) (1973) 235–236.

[9] C.D.G. King, Heat transfer and pressure drop for an air–water mixture flowing in a 0.737 inch I.D. horizontal tube, M.S. Thesis, Mechanical Engineering Department, University of California, Berkeley, CA, 1952.

[10] R.H. Pletcher, An experimental and analytical study of heat transfer and pressure drop in horizontal annular two-phase, two-component flow, Ph.D. Thesis, Cornell University, Ithaca, NY, 1966.

[11] Y. Taitel, A.E. Dukler, A model for predicting flow regime transitions in horizontal and near horizontal gas–liquid flow, AIChE J. 22 (1) (1976) 47–54.

[12] M.E. Ewing, J.J. Weinandy, R.N. Christensen, Observations of two-phase flow patterns in a horizontal circular channel, Heat Transfer Eng. 20 (1) (1999) 9–14.

[13] S.S. Yoo, Heat transfer and friction factors for non-Newtonian fluids in turbulent pipe flow, Ph.D. Thesis, University of Illinois at Chicago Circle, IL, 1974.

[14] D. Kim, An experimental and empirical investigation of convective heat transfer for gas–liquid two-phase flow in vertical and horizontal pipes, Ph.D. Thesis, School of Mechanics and Aerospace Engineering, Oklahoma State University, Stillwater, OK, 2000.

[15] A.J. Ghajar, Y.H. Zurigat, Microcomputer-assisted heat transfer measurement/analysis in a circular tube, Int. J. Appl. Eng. Ed. 7 (2) (1991) 125–134.

[16] A.P. Colburn, A method of correlating forced convection heat transfer data and a comparison with liquid friction, Trans. Am. Inst. Chem. Eng. 29 (1933) 174–210.

[17] V. Gnielinski, New equations for heat and mass transfer in turbulent pipe and channel flow, Int. Chem. Eng. 16 (2) (1976) 359–368.

[18] A.J. Ghajar, T.M. Tam, Heat transfer measurements and correlations in the transition region for a circular tube with three different inlet configurations, Exp. Thermal Fluid Sci. 8 (1994) 79–90.

[19] S.J. Kline, F.A. McClintock, Describing uncertainties in single-sample experiments, Mech. Eng. 1 (1953) 3–8.

[20] G. Breber, J.W. Palen, J. Taborek, Prediction of horizontal tubeside condensation of pure components using flow regime criteria, J. Heat Transfer 102 (1980) 471–476.

[21] G.W. Govier, K. Aziz, The Flow of Complex Mixtures in Pipes, Van Nostrand Reinhold, New York, 1973.

[22] P. Griffith, G.B. Wallis, Two-phase slug flow, J. Heat Transfer, Trans. ASME, Ser. C 83 (1961) 307–320.

[23] G.F. Hewitt, N.S. Hall-Taylor, Annular Two-Phase Flow, Pergamon Press, Oxford, 1970.

[24] D. Barnea, Y. Luninski, Y. Taital, Flow pattern in horizontal and vertical two phase flow in small diameter pipes, Can. J. Chem. Eng. 61 (1983) 617–620.

[25] V.P. Carey, Liquid–Vapor Phase-Change Phenomena: An Introduction to the Thermophysics of Vaporization and Condensation Process in Heat Transfer Equipment, Taylor & Francis, Bristol, 1992.

[26] A.J. Zaidi, G.E. Sims, The effect of a surfactant on flow patterns, pressure drop and heat transfer in two-phase two-component vertical flow, in: C.L. Tien, V.P. Carey, J.K. Ferrell (Eds.), Presented at the 8th International Heat Transfer Conference, San Francisco, CA, vol. 5, Hemisphere, Washington, DC, 1986, pp. 2283–2288.

[27] A.A. Kudirka, R.J. Grosh, P.W. McFadden, Heat transfer in two-phase flow of gas–liquid mixtures, I & EC Fundament. 4 (3) (1965) 339–344.

[28] H. Groothuis, W.P. Hendal, Heat transfer in two-phase flow, Chem. Eng. Sci. 11 (1959) 212–220.

[29] S.R. Ravipudi, T.M. Godbold, The effect of mass transfer on heat transfer rates for two-phase flow in a vertical pipe, Presented at the 6th International Heat Transfer Conference, Toronto, vol. 1, 1978, pp. 505–510.

[30] R.H. Pletcher, H.N. McManus Jr., Heat transfer and pressure drop in horizontal annular two-phase, two-component flow, Int. J. Heat Mass Transfer 11 (1968) 1087–1104.